Research Article | Vol. 24, No. 26 | 26 Dec 2016 | OPTICS EXPRESS 29984

Optics EXPRESS

Complex effective index in graphene-silicon waveguides

V. SORIANELLO,[1] G. DE ANGELIS,[2] T. CASSESE,[2] M. MIDRIO,[3] M. ROMAGNOLI,[1,*] M. MOSHIN,[4] M. OTTO,[4] D. NEUMAIER,[4] I. ASSELBERGHS,[5] J. VAN CAMPENHOUT,[5] AND C. HUYGHEBAERT[5]

[1]*Consorzio Nazionale per le Telecomunicazioni (CNIT), National Laboratory of Photonic Networks, Via G. Moruzzi 1, 56124 Pisa, Italy*
[2]*Tecip Institute - Scuola Superiore Sant'Anna, Via G. Moruzzi 1, 56124 Pisa, Italy*
[3]*Consorzio Nazionale per le Telecomunicazioni (CNIT), University of Udine, Via delle Scienze 206, 33100 Udine, Italy*
[4]*Advanced Microelectronic Center Aachen (AMICA), Applied Micro and Optoelectronic (AMO) GmbH, Otto-Blumenthalstr. 25, 52074 Aachen, Germany*
[5]*IMEC, Kapeldreef 75, 3001 Leuven, Belgium*
**marco.romagnoli@cnit.it*

Abstract: We report for the first time and characterize experimentally the complex optical conductivity of graphene on silicon photonic waveguides. This permits us to predict accurately the behavior of photonic integrated devices encompassing graphene layers. Exploiting a Si microring add/drop resonator, we show the effect of electrical gating of graphene on the complex effective index of the waveguide by measuring both the wavelength shift of the resonance and the change in the drop peak transmission. Due to electro-refractive effect of graphene a giant ($>10^{-3}$) change in the effective index is demonstrated for the first time on Si photonics waveguides and this large effect will crucially impact performances and consumption of Si photonics devices. We confirmed the results by two independent experiments involving two different gating schemes: Si gating through the ridge waveguide, and polymer-electrolyte gating. Both the experiments demonstrate a very large phase effect in good agreement with numerical calculations. The reported results validate the Kubo model for the case of graphene-Si photonics interfaces and for propagation in this type of waveguide. This is fundamental for the next design and fabrication of future graphene-silicon photonics devices.

© 2016 Optical Society of America

OCIS codes: (250.5300) Photonic integrated circuits; (230.0250) Optoelectronics; (130.3120) Integrated optics devices; (260.2110) Electromagnetic optics

References and links

1. G. T. Reed and A. Knight, *Silicon Photonics: An Introduction* (J. Wiley & Sons Ltd, 2004).
2. R. Soref, "The past, present and future of Silicon photonics," IEEE J. Sel. Top. Quantum Electron. **12**(6), 1678–1687 (2006).
3. B. Jalali and S. Fathpour, "Silicon photonics," J. Lightwave Technol. **24**(12), 4600–4615 (2007).
4. Y. Arakawa, T. Nakamura, Y. Urino, and T. Fujita, "Silicon photonics for next generation system integration platform," IEEE Commun. Mag. **51**(3), 72–77 (2013).
5. L. Pavesi and D. J. Lockwood, *Silicon Photonics III*, (Springer Verlag, 2016).
6. R. A. Soref and J. P. Lorenzo, "All-Silicon active and passive guided wave components for λ = 1.3 and 1.6μm," IEEE J. Quantum Electron. **22**(6), 873–879 (1986).
7. G. T. Reed, *Silicon Photonics: The State of the Art*, (J. Wiley & Sons Ltd, 2008).
8. M. Liu, X. Yin, E. Ulin-Avila, B. Geng, T. Zentgraf, L. Ju, F. Wang, and X. Zhang, "A Graphene-based broadband optical modulator," Nature **474**(7349), 64–67 (2011).
9. M. Liu, X. Yin, and X. Zhang, "Double-layer Graphene optical modulator," Nano Lett. **12**(3), 1482–1485 (2012).
10. C. T. Phare, Y. D. Lee, J. Cardenas, and M. Lipson, "Graphene electro-optic modulator with 30 GHz bandwidth," Nat. Photonics **9**(8), 511–514 (2015).

#275895 http://dx.doi.org/10.1364/OE.24.029984
Journal © 2016 Received 30 Sep 2016; revised 26 Nov 2016; accepted 27 Nov 2016; published 16 Dec 2016

Optics EXPRESS

11. Y. Hu, M. Pantouvaki, J. Van Campenhout, S. Brems, I. Asselberghs, C. Huyghebaert, P. Absil, and D. Van Thourhout, "Broadband 10 Gb/s operation of graphene electro-absorption modulator on silicon," Laser Photonics Rev. **10**(2), 307–316 (2016).
12. C. Xu, Y. Jin, L. Yang, J. Yang, and X. Jiang, "Characteristics of electro-refractive modulating based on Graphene-Oxide-Silicon waveguide," Opt. Express **20**(20), 22398–22405 (2012).
13. J. Gosciniak and D. T. H. Tan, "Theoretical investigation of graphene-based photonic modulators," Sci. Rep. **3**, 1897 (2013).
14. M. Mohsin, D. Neumaier, D. Schall, M. Otto, C. Matheisen, A. L. Giesecke, A. A. Sagade, and H. Kurz, "Experimental verification of electro-refractive phase modulation in Graphene," Sci. Rep. **5**, 10967 (2015).
15. A. Phatak, Z. Cheng, C. Qin, and K. Goda, "Design of electro-optic modulators based on Graphene-on-Silicon slot waveguides," Opt. Lett. **41**(11), 2501–2504 (2016).
16. Y. M. Zuev, W. Chang, and P. Kim, "Thermoelectric and magnetothermoelectric transport measurements of graphene," Phys. Rev. Lett. **102**(9), 096807 (2009).
17. P. Wei, W. Bao, Y. Pu, C. N. Lau, and J. Shi, "Anomalous thermoelectric transport of Dirac particles in graphene," Phys. Rev. Lett. **102**(16), 166808 (2009).
18. F. Xia, T. Mueller, Y. M. Lin, A. Valdes-Garcia, and P. Avouris, "Ultrafast graphene photodetector," Nat. Nanotechnol. **4**(12), 839–843 (2009).
19. T. Mueller, F. N. Xia, and P. Avouris, "Graphene photodetectors for high-speed optical communications," Nat. Photonics **4**(5), 297–301 (2010).
20. R. J. Shiue, Y. Gao, Y. Wang, C. Peng, A. D. Robertson, D. K. Efetov, S. Assefa, F. H. L. Koppens, J. Hone, and D. Englund, "High-responsivity graphene–boron nitride photodetector and autocorrelator in a silicon photonic integrated circuit," Nano Lett. **15**(11), 7288–7293 (2015).
21. A. Majumdar, J. Kim, J. Vuckovic, and F. Wang, "Electrical control of silicon photonic crystal cavity by graphene," Nano Lett. **13**(2), 515–518 (2013).
22. X. Gan, R. J. Shiue, Y. Gao, K. F. Mak, X. Yao, L. Li, A. Szep, D. Walker, Jr., J. Hone, T. F. Heinz, and D. Englund, "High-contrast electrooptic modulation of a photonic crystal nanocavity by electrical gating of graphene," Nano Lett. **13**(2), 691–696 (2013).
23. V. Sorianello, M. Midrio, and M. Romagnoli, "Design optimization of single and double layer Graphene phase modulators in SOI," Opt. Express **23**(5), 6478–6490 (2015).
24. C. W. Chen, F. Ren, G. C. Chi, S. C. Hung, Y. P. Huang, J. Kim, I. Kravchenko, and S. J. Pearton, "Effects of semiconductor processing chemicals on conductivity of Graphene," J. Vac. Sci. Technol. B **30**(4), 040602 (2012).
25. J. Chan, A. Venugopal, A. Pirkle, S. McDonnell, D. Hinojos, C. W. Magnuson, R. S. Ruoff, L. Colombo, R. M. Wallace, and E. M. Vogel, "Reducing extrinsic performance-limiting factors in Graphene grown by chemical vapor deposition," ACS Nano **6**(4), 3224–3229 (2012).
26. A. Pirkle, J. Chan, A. Venugopal, D. Hinojos, C. W. Magnuson, S. McDonnell, L. Colombo, E. M. Vogel, R. S. Ruoff, and R. M. Wallace, "The effect of chemical residues on the physical and electrical properties of chemical vapor deposited Graphene transferred to SiO2," Appl. Phys. Lett. **99**(12), 122108 (2011).
27. Z. Cheng, Q. Zhou, C. Wang, Q. Li, C. Wang, and Y. Fang, "Toward intrinsic Graphene surfaces: a systematic study on thermal annealing and wet-chemical treatment of SiO2-supported Graphene devices," Nano Lett. **11**(2), 767–771 (2011).
28. S. Ryu, L. Liu, S. Berciaud, Y. J. Yu, H. Liu, P. Kim, G. W. Flynn, and L. E. Brus, "Atmospheric oxygen binding and hole doping in deformed Graphene on a SiO_2 substrate," Nano Lett. **10**(12), 4944–4951 (2010).
29. J. H. Chen, C. Jang, S. Xiao, M. Ishigami, and M. S. Fuhrer, "Intrinsic and extrinsic performance limits of Graphene devices on SiO2," Nat. Nanotechnol. **3**(4), 206–209 (2008).
30. Y. C. Chang, C. H. Liu, C. H. Liu, Z. Zhong, and T. B. Norris, "Extracting the complex optical conductivity of mono- and bilayer Graphene by ellipsometry," Appl. Phys. Lett. **104**(26), 261909 (2014).
31. P. P. Absil, P. De Heyn, H. Chen, P. Verheyen, G. Lepage, M. Pantouvaki, J. De Coster, A. Khanna, Y. Drissi, D. Van Thourhout, and J. Van Campenhout, "Imec iSiPP25G Silicon photonics: a robust CMOS-based photonics technology platform," Proc. SPIE **9367**, 93670V (2015).
32. X. Li, W. Cai, J. An, S. Kim, J. Nah, D. Yang, R. Piner, A. Velamakanni, I. Jung, E. Tutuc, S. K. Banerjee, L. Colombo, and R. S. Ruoff, "Large-area synthesis of high-quality and uniform Graphene films on Copper foils," Science **324**(5932), 1312–1314 (2009).
33. Graphenea, "Graphenea granted patent on graphene transfer," http://www.graphenea.com/blogs/graphene-news/16922317-graphenea-granted-patent-on-graphene-transfer.
34. M. Politou, I. Asselberghs, I. Radu, T. Conard, O. Richard, C. S. Lee, K. Martens, S. Sayan, C. Huyghebaert, Z. Tokei, S. De Gendt, and M. Heyns, "Transition metal contacts to Graphene," Appl. Phys. Lett. **107**(15), 153104 (2015).
35. S. Das Sarma, S. Adam, E. H. Hwang, and E. Rossi, "Electronic transport in two-dimensional Graphene," Rev. Mod. Phys. **83**(2), 407–470 (2011).
36. Y. W. Tan, Y. Zhang, K. Bolotin, Y. Zhao, S. Adam, E. H. Hwang, S. Das Sarma, H. L. Stormer, and P. Kim, "Measurement of scattering rate and minimum conductivity in Graphene," Phys. Rev. Lett. **99**(24), 246803 (2007).
37. H. A. Haus, M. A. Popović, M. R. Watts, and C. Manolatou, "Optical resonators and filters," in *Optical Microcavities*, K. Vahala, ed. (World Scientific Publishing, 2004).

Optics EXPRESS

38. W. Bogaerts, P. De Heyn, T. Van Vaerenbergh, K. De Vos, S. K. Selvaraja, T. Claes, P. Dumon, P. Bienstman, D. Van Thourhout, and R. Baets, "Silicon microring resonators," Laser Photonics Rev. **6**(1), 47–73 (2012).
39. D. K. Efetov and P. Kim, "Controlling electron-phonon interactions in Graphene at ultrahigh carrier densities," Phys. Rev. Lett. **105**(25), 256805 (2010).

1. Introduction

Silicon (Si) photonics is a technology mostly considered for miniaturization and for high volume manufacturing of photonics integrated circuits. Si photonics includes passive functionalities, as for instance waveguides, and active functionalities, as modulation, switching, tuning and detection [1–5]. In the active Si photonics devices the basic mechanisms to induce absorption or, more importantly, index change are the plasma dispersion effect or the thermo-optical effect (the last for the index variation only). Plasma dispersion originates from a change of the free carrier density (injection, depletion or accumulation) in Si doped regions, in particular the index change mostly depends on hole density variations [6]. Depending on the carrier modulation mechanism, this effect can be used to change the refractive index of Si up to $\Delta n = 10\text{-}3$ for a carrier modulation of the order of 5e17cm-3. However, such large changes are achievable only in Si waveguide based on the injection or accumulation of free carriers. In the case of injection the index variation may be large but the response is very slow (1ns) because limited by carrier diffusion in the depletion region. In the case of carrier accumulation instead, the change in index is large but the modulator is limited by the insertion loss due to polySi upper part of the waveguide [7]. Typical Si photonics phase modulators requiring >20GHz bandwidth and low insertion loss, are based on the carrier depletion effect in reverse biased pn junction. These can be extremely fast (<<ns) but the waveguide index change is only of order $\Delta n = 10\text{-}4$ at 1550nm [1]. This lower value is mainly associated to the maximum reverse bias that can be applied to the pn junction in order to avoid breakdown. Conversely, the thermo-optical effect can lead to a larger effect on the index change thanks to the large thermo-optic coefficient of Si ($\Delta n/\Delta T = 1.8\text{x}10^{-4}$/K) [1], however the thermo optical effect is much slower (μs scale).

Graphene is a 2D material with quite interesting dielectric properties which can be combined as active material with Si photonics in order to provide both very efficient light modulation and detection [8–20]. Earlier experiments demonstrated, by a vertical illumination method, that graphene placed on top of a Si structure (e.g. photonic crystal) can induce changes in both absorption and index of refraction [21, 22]. Example of graphene on Si waveguide modulators have been reported either based on experiments or based on design [8–15, 23]. The theoretical approach is based on the Kubo model that does not specifically include the interface with the supporting waveguide material, e.g. the silicon waveguide or its cladding oxide. This interface may affect the dielectric properties of graphene, in fact dangling bonds, impurities, defects, may induce a reduction in conductivity and in carrier mobility and consequently leading to an increase of electrical resistivity and optical background loss [24–29]. For this reason, the characterization of the real and imaginary part of graphene on Si waveguide effective index and the theoretical fitting is important for the design of an integrated photonic device.

In this paper, we report the first complete demonstration and characterization of the complex conductivity of graphene in a Si-photonics waveguide. We obtain an excellent agreement with theoretical fitting based on the use of Kubo formula. This is a fundamental result for accurate design of integrated photonic devices encompassing Graphene. The characterization was done by means of an add/drop microring resonator based on Si ridge waveguides integrated with a single layer of graphene placed on top of the waveguide core. We measured peak transmissions and wavelength shift of the resonance at the through and drop ports of the microring as a function of the graphene gating. The wavelength shift corresponds to a change of effective index larger than 10-3, i.e. almost 30 times more than the typical shift achievable with plasma dispersion effect in Si p-n junctions used in depletion mode [1,6]. We remark that even though a very weak electro-refraction of Graphene on top of

Optics EXPRESS

a Si-photonics waveguide has been previously observed [14], to the best of our knowledge this is the first time that a giant change of refractive index of more than 10^{-3} is experimentally shown on a silicon photonics waveguide, using an effect capable for multi GHz operation. The observation of the very large electro-refractive effect crucially impacts on the possibility to scale in performance and consumption the Si-Photonics roadmap.

The characterization has been carried out with two different graphene gating schemes and the results were consistent. Full characterization of absorption and index of refraction in a large doping range (Fermi energy from 0eV up to 0.8eV) of the graphene were compared with the theoretical model. In particular, we used a simplified closed formula for the optical conductivity of graphene derived from the Kubo model [23,30]. The results confirm the validity of the simplified model and provide a highlight on the relevance of the silicon/graphene interface for the design of an optical device. In addition, measurements indicate the quality of the graphene layer transferred on top of the Si waveguide showing a carrier scattering time of 25fs.

2. Fabrication

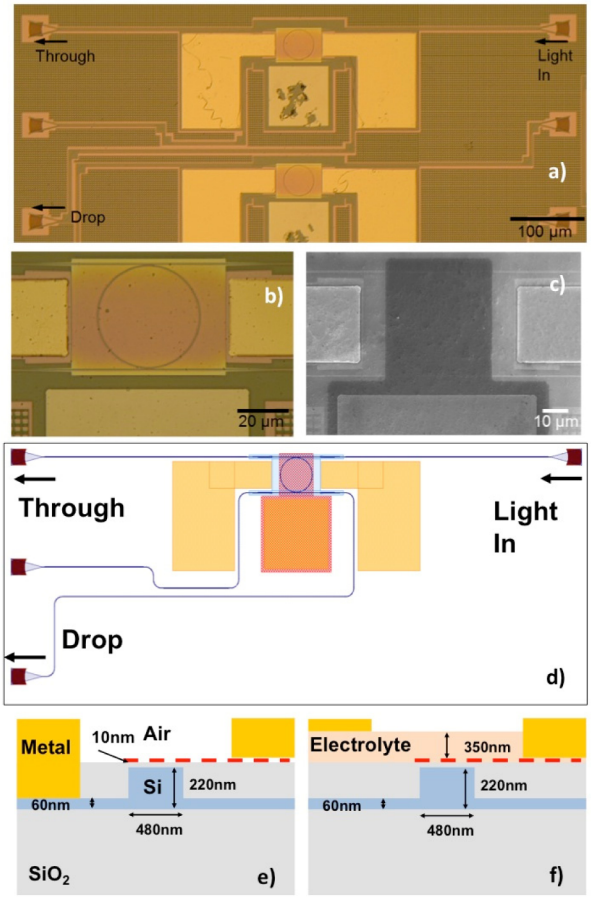

Fig. 1. Optical micrograph of the fabricated device (a). Detail of the microring resonator (b). SEM image of the Graphene covered microring resonator (c). Device layout (d). Cross sections for two different gating schemes: Si gating (e), Electrolyte gating (f).

Figure 1 shows optical micrographs of the fabricated device (a-b), a SEM image of the microring covered with Graphene (c), the device layout (d) and schematic cross section for two possible gating schemes: Graphene gating through the Si ridge waveguide (e) and

Optics EXPRESS

Graphene gating by means of a polymer-electrolyte (f). With reference to Fig. 1(d) and assuming an input light propagating from left to right, we define: the input port (light in), the through port collecting the light that does not resonate in the ring and the drop port collecting the resonating wavelength. The microring is based on a ridge waveguide with 60nm slab and a core cross-section 480nm x 220nm on standard silicon on insulator (SOI) platform with 220 nm Si over-layer and 2 µm buried oxide (BOX). We did not include doping in the waveguide in order to avoid intrinsic losses in the Si microring, while the slab region is highly p-doped up to 1µm distance from the core. The SiO_2 top cladding is thinned down to the waveguide top edge. The graphene layer is placed on top of the Si waveguide separated by a 10nm spacer of a high quality thermal SiO_2. This way a Si-SiO_2-graphene capacitor is realized in order to access electrical gating of graphene through the Si waveguide. In particular, Si gating is achieved through metal contacts on the Si slab and on the graphene layer as shown in Fig. 1(e). On the contrary, in the experiment with electrolyte gating, the potential was applied to the electrolyte keeping the graphene contact at ground potential. The electrolyte consisted of poly(ethylene oxide) and lithium perchlorate (PEO:$LiClO_4$ in ratio 9:1) and was spin-coated (thickness ~350nm) and then baked for 10 sec at 100 °C to evaporate excess solvent.

The device was fabricated at IMEC in a standard SOI photonic platform [31]. The microring radius is 20µm with an expected free spectral range of 4.8nm, while the distance between the bus waveguide to the microring is 180nm. Graphene growth and transfer was performed at Graphenea according to their standard method. Graphene was grown by chemical vapor deposition (CVD) on copper foils and then transferred with the wet method to our Si samples [32]. Details on Graphenea growth and transfer processes can be found in [33].

Figure 2 shows the Raman spectrum of graphene in the central part of the silicon microring (left panel) and the I_{2D}/I_G mapping in the whole area of the microring, showing clearly that graphene is monolayer. The blue spots within the yellowish region are probably bilayer islands and folds in the graphene. Also, observe that I_{2D}/I_G depends on the underlying substrate. This explains the lower values on the waveguide/ring and above and below the two horizontal waveguides.

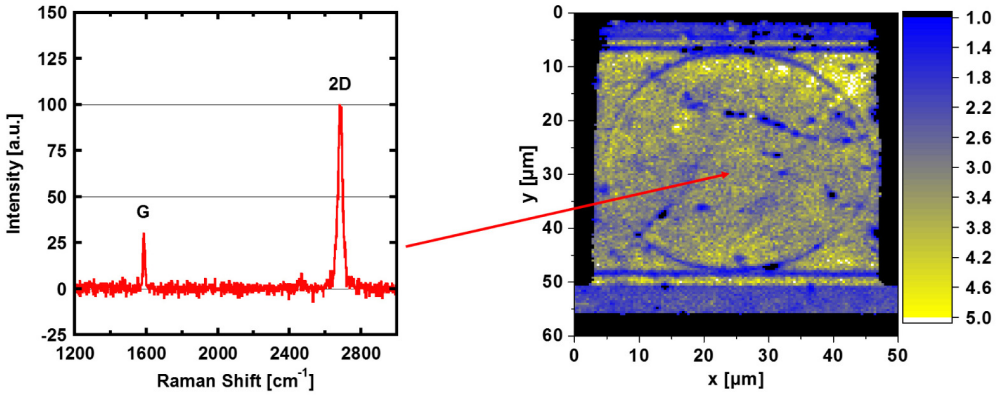

Fig. 2. Left panel: Raman spectrum of graphene in the central part of the silicon microring. Right panel: I2D/IG mapping of graphene in the area of the silicon microring.

Further device processing was done using conventional photolithography techniques. A bilayer resist layer stack of PMMA / IX845 was used for channel patterning and graphene etch was done using conventional O_2-plasmas. Graphene metal contact and Si contact were processed in two consecutive metallization steps. A Pd (50nm) contact has been implemented on top of the graphene layer [34], while the Si contact consists of a Ti (20nm) /Pt (20nm) /Au (30nm) stack deposited after an HF to remove the native SiO_2.

Optics EXPRESS

3. Theoretical analysis

We used a commercially available mode solver to evaluate the effective index, the group index and the optical absorption of the waveguides at a center wavelength of 1.55μm for different values of the graphene Fermi level energy. Graphene has been modeled with in-plane dielectric constant obtained from the optical conductivity as discussed in [23], while the out-of-plane dielectric constant has been set equal to the graphite dielectric constant. In particular, we used the closed formula for the complex optical conductivity [30]:

$$\sigma(\omega)=\frac{\sigma_0}{2}\left(\tanh\frac{\hbar\omega+2\mu_C}{4k_BT}+\tanh\frac{\hbar\omega-2\mu_C}{4k_BT}\right)-i\frac{\sigma_0}{2\pi}\ln\left[\frac{(\hbar\omega+2\mu_C)^2}{(\hbar\omega-2\mu_C)^2+(2k_BT)^2}\right]+i\frac{4\sigma_0}{\pi}\frac{\mu_C}{\hbar\omega+i\hbar\gamma} \quad (1)$$

Here $\sigma_0 = q^2/(4\hbar)$ is the universal conductivity of graphene (with q the electron charge), μ_C is the Fermi level, k_BT the thermal energy, $\hbar\omega$ the photon energy and $\hbar\gamma$ the electron relaxation energy, with $\gamma = 1/\tau$ the intraband scattering rate. The physical mechanisms affecting the intraband scattering stems primarily from long-range scattering [35]. In this study, we do not investigate on these mechanisms. Moreover, the intraband scattering term (last term in Eq. (1)) sets in when the Fermi level is larger than the optical energy, i.e. for large carrier density. In these conditions, the scattering time can be treated as a macroscopic constant. In the numerical calculations, we considered three different state-of-the-art values of the intra-band relaxation time τ = 10fs, 50fs and 100fs in order to take into account different qualities of graphene [30,36]. Figure 3 shows the effective index and absorption versus the graphene chemical potential (μc) for the Si waveguides shown in Fig. 1 at 1.55μm.

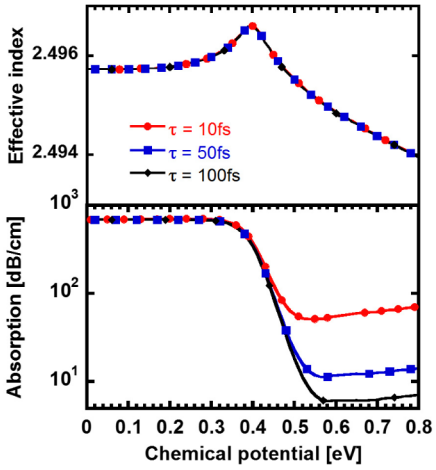

Fig. 3. Effective index (top) and absorption (bottom) of the graphene integrated Si waveguide at 1.55μm versus chemical potential in graphene.

When the graphene Fermi level energy is below half the photon energy (0.4eV at 1.55μm), we observe a strong optical absorption due to the interband transition while when the Fermi level energy exceeds half the photon energy the optical absorption drops down and bounds to a minimum level that is determined by the intraband scattering mechanisms.

In the proposed device, the microring transmission will be affected by the change in effective index and absorption in two ways. The first is related to the absorption: if the single round-trip loss is large enough, waves no longer coherently add inside the ring and the ring resonance is suppressed [37]. In this case, light is transmitted to the through port with a minimum insertion loss due to the light coupled from the input waveguide to the resonator, which is absorbed in the ring path. Conversely, in the low loss condition, i.e. when the graphene Fermi level energy exceeds half of the photon energy, the microring transmission at

Optics EXPRESS

the through port and at the drop port will exhibit the expected resonances. Along with the change in absorption, the corresponding change in refractive index will affect the resonance as well, i.e. by tuning μ_c the resonance wavelength will experience a shift. In particular, the resonance wavelength is directly proportional to the effective index of the waveguide [38]. With reference to Fig. 1, when the Fermi level energy increases from the Dirac point ($\mu_c = 0$ eV) the effective index increases inducing a red shift of the resonance wavelength. However, when the Fermi energy exceeds half of the photon energy the effective index decreases and the resonance will show blue shift towards shorter wavelengths.

4. Experimental results

We used a tunable laser in the C-band to characterize the microring transmission spectra at the through and drop ports of Fig. 1(a) at different gating voltages. Light was in- and out-coupled to the chip through grating couplers provided by the chosen Si photonic platform with an expected insertion loss of 3dB to 5dB per coupler [34]. We gated graphene with the schemes of Fig. 1(e) and 1(f): through the Si slab and through the electrolyte. The first option is the one enabling the integration of graphene in the Si photonics platform and it is CMOS compatible. The second option is widely used for basic characterization purposes as it allows very high doping of the graphene layer, i.e. Fermi energy larger than 0.6 eV. Figure 4(a) and 3(b) shows the measured spectra when gating with Si and electrolyte, respectively.

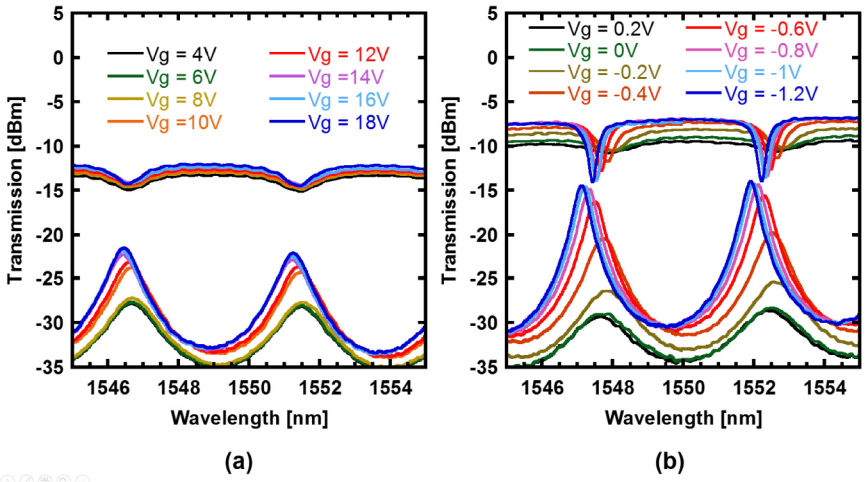

Fig. 4. Microring through and drop transmission spectra at different voltages for Si (a) and electrolyte gating (b).

As expected by tuning the graphene Fermi energy with electrical gating the resonance amplitude and position changes. The main differences between the two experiments are the value of the gating voltage, and the maximum achievable tuning. In particular, in the Si gating experiment the voltage was much larger than in the electrolyte gating experiment. This was attributed to parasitic effects due to the non-ideal behavior of the Si-SiO_2-graphene gating capacitor. In particular, we observed leakage currents in the order of hundreds of nA, which are responsible of large voltage drops in the Si undoped regions and in the ungated graphene, which are highly resistive. Moreover, the leakage current increased for gating voltage larger than 20V, this prevented from achieving the low propagation loss condition at large graphene doping because carriers did not accumulate on the capacitor arms, but are swept away by the leakage current. Such impairment can be avoided by reducing the series resistance of the device. For example, a light doping of the Si waveguide and an optimized geometry for the graphene layer will reduce the voltage drop on the undesired regions so that the voltage applied to the device is entirely applied on the capacitor [11]. Conversely, in the electrolyte

Optics EXPRESS

gated experiment we successfully reached the low propagation loss condition thanks to the very high doping achievable with such technique [39]. In both the experiments we also observed a slight misalignment between the through and drop transmission spectra. In the Si-SiO_2-graphene capacitor, this was attributed to hysteresis effects in cycling the applied voltage. Hysteresis can be avoided by suitably discharging the graphene capacitor. In the experiment with electrolyte, the shift is caused by a small environmental temperature drift during measurement.

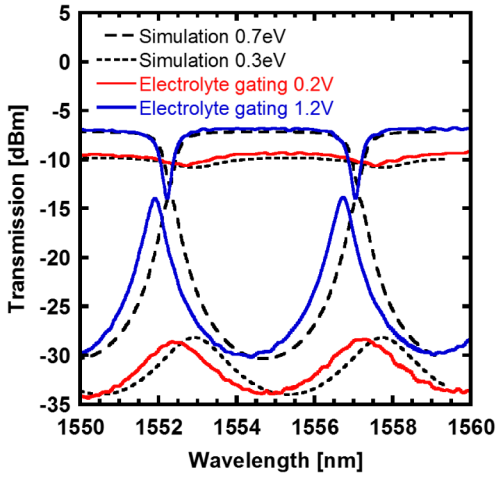

Fig. 5. Experimental through and drop transmission spectra at two different gating voltage (solid line) compared to numerical simulations (dashed lines).

In the Si gating experiment, we observed larger optical losses respect to the electrolyte gated experiment. This is attributed to the different experimental setups. Moreover, the two devices are covered with different top claddings in the two experiments, leading to different insertion losses. In particular, the grating couplers provided by the Si photonic platform were designed for a SiO_2 top cladding. However, in the Si gating experiment the chip was air cladded; while in the electrolyte gating experiment the polymer (refractive index 1.6 acted as top cladding). Because of the difference in cladding, the grating coupler was suitable for the electrolyte scheme but more lossy for the Si gated case.

We used the curves from the electrolyte experiments to fit the experimental data with the numerical simulations. In fact, the larger range of achievable dopings allowed the fit between the voltage dependent experimental curves and the simulations done versus the Fermi level energy. Figure 5 shows the experimental through and drop port spectra at 0.2V and 1.2V corresponding to high and low propagation loss, respectively, and the corresponding simulated curves obtained using Eq. (1). From this numerical fitting, we could extract the relation between the applied voltages and the chemical potential. Based on the fitting of the experimentally obtained transmission data by the theoretical model we extracted a capacitance of 4 $\mu F/cm^2$ for the electrolyte gate. In this fitting procedure, the gate capacitance was the only open fitting parameter. The numerical model successfully fitted the experiment with a scattering parameter of 25fs. As discussed above the drop curves exhibit a shift in wavelength with respect to the through port because of the hysteresis effect. In particular, the through port was measured first (for all voltages) and then the drop port in both experiments.

Figure 6 shows the expected wavelength shift at the drop port (a) and peak transmission change (b) as a function of the graphene chemical potential compared to the extracted experimental results of the two gating schemes. The peak transmission change is normalized to the minimum peak transmission in both the experiments to cope with the different experimental conditions of the optical setups. In Fig. 6(b) we reported the numerical

Optics EXPRESS

simulations for different scattering parameters (10, 25 and 100fs) to show the relevant dependence on this parameter in the transparency region. The experimental results are in good agreement with the simulations validating the used numerical model based on Eq. (1). Observe, in particular, the similarity between the measured resonance frequency shift of Fig. 6(a) and the simulated results of the top panel of Fig. 3.

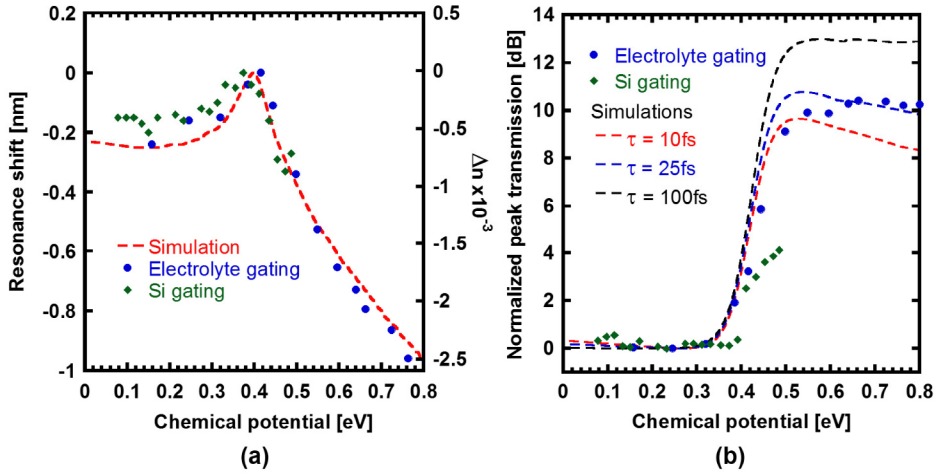

Fig. 6. Extracted resonance shift and effective index change (a) calculated with Eq. (2) versus chemical potential. Peak transmission change versus chemical potential (b). In both figures, the dashed lines represent the numerical simulations while the green diamonds and the blue dots represent the experimental values extracted from the Si gating and electrolyte gating experiments respectively.

This is the first time, up to our knowledge, that an experimental verification of the refractive and absorptive properties of graphene on Si photonics waveguide have been experimentally characterized and fitted. This is also a direct demonstration of the strong phase effect induced by graphene on Si waveguide effective index. In fact, we demonstrated a phase shift of 0.35 nm in the Si gating experiment and more than 1 nm in the electrolyte gating experiment with respect to the maximum effective index at 0.4 eV. From these results, we can extract the effective index change Δn_{eff} as [38]:

$$\Delta n_{eff} = \frac{\Delta\lambda_{res} \cdot n_g}{\lambda_{res}} \tag{2}$$

where $\Delta\lambda_{res}$ is the resonance shift, n_g is the waveguide group index and λ_{res} is the original wavelength of the resonance. From dispersive simulations we evaluated $n_g = 4.05$ for the proposed waveguide. Hence, we could evaluate the effective index change for the two experiments: 9×10^{-4} for the Si gating experiment and 2.6×10^{-3} for the electrolyte gating. These results are reported on the right axes of Fig. 6(b) and are consistent with the effective index change of Fig. 3(a) and up to 30 times larger than the typical phase shift achievable with plasma dispersion effect in Si p-n junctions used in depletion mode [1].

5. Conclusions

In conclusion, we experimentally observed the tuning of the complex optical properties of graphene on Si photonic waveguides. Through the characterization of a Si microring resonator, we experimentally verified the electrically induced change of both absorption and refractive index of graphene. The experimental results are in very good agreement with the numerical simulation of the proposed device performed by integrating the closed formula of

Optics EXPRESS

the optical conductivity in a commercially available mode solver. The reported results set a base of data for the next design and fabrication of future graphene-silicon photonics devices.

Funding

European Commission (696656).

80.183.24.230 {ts '2016-12-16 12:19:36'}